BRAIN
A JOURNAL OF NEUROLOGY

REPORT

Bi-allelic variants in HOPS complex subunit VPS41 cause cerebellar ataxia and abnormal membrane trafficking

Leslie E. Sanderson,[1,†] Kristina Lanko,[1,†] Maysoon Alsagob,[2,3,†] Rawan Almass,[2,4,†] Nada Al-Ahmadi,[2,5,†] Maryam Najafi,[6,7] Mohammad A. Al-Muhaizea,[8,‡] Hamad Alzaidan,[4,‡] Hesham AlDhalaan,[8,‡] Elena Perenthaler,[1] Herma C. van der Linde,[1] Anita Nikoncuk,[1] Nikolas A. Kühn,[1] Dinu Antony,[7] Tarek Mustafa Owaidah,[9] Salmo Raskin,[10] Luana Gabriela Dalla Rosa Vieira,[11] Romulo Mombach,[12] Najmeh Ahangari,[13] Tainá Regina Damaceno Silveira,[14] Najim Ameziane,[14] Arndt Rolfs,[14,15] Aljohara Alharbi,[9] Raghda M. Sabbagh,[9] Khalid AlAhmadi,[8] Bashayer Alawam,[4] Hazem Ghebeh,[16] Aljouhra AlHargan,[2] Anoud A. Albader,[2] Faisal S. Binhumaid,[2] Ewa Goljan,[2] Dorota Monies,[2] Osama M. Mustafa,[2] Mazhor Aldosary,[2] Albandary AlBakheet,[2] Banan Alyounes,[2] Faten Almutairi,[2] Ali Al-Odaib,[2] Durdane Bekar Aksoy,[17] A. Nazli Basak,[18] Robin Palvadeau,[18] Daniah Trabzuni,[19] Jill A. Rosenfeld,[20] Ehsan Ghayoor Karimiani,[21,22] Brian F. Meyer,[2,23,24] Bedri Karakas,[25] Futwan Al-Mohanna,[26] Stefan T. Arold,[27,28] Dilek Colak,[29] Reza Maroofian,[30] Henry Houlden,[30] Aida M. Bertoli-Avella,[14] Miriam Schmidts,[6,7,§] Tahsin Stefan Barakat,[1,§] Tjakko J. van Ham[1,§] and Namik Kaya[2,24,§]

†,‡,§These authors contributed equally to this work.

Membrane trafficking is a complex, essential process in eukaryotic cells responsible for protein transport and processing. Deficiencies in vacuolar protein sorting (VPS) proteins, key regulators of trafficking, cause abnormal intracellular segregation of macromolecules and organelles and are linked to human disease. VPS proteins function as part of complexes such as the homotypic fusion and vacuole protein sorting (HOPS) tethering complex, composed of VPS11, VPS16, VPS18, VPS33A, VPS39 and VPS41. The HOPS-specific subunit VPS41 has been reported to promote viability of dopaminergic neurons in Parkinson's disease but to date has not been linked to human disease. Here, we describe five unrelated families with nine affected individuals, all carrying homozygous variants in VPS41 that we show impact protein function. All affected individuals presented with a progressive neurodevelopmental disorder consisting of cognitive impairment, cerebellar atrophy/hypoplasia, motor dysfunction with ataxia and dystonia, and nystagmus. Zebrafish disease modelling supports the involvement of VPS41 dysfunction in the disorder, indicating lysosomal dysregulation throughout the brain and providing support for cerebellar and microglial abnormalities when *vps41* was mutated. This provides the first example of human disease linked to the HOPS-specific subunit VPS41 and suggests the importance of HOPS complex activity for cerebellar function.

1 Department of Clinical Genetics, Erasmus MC University Medical Center, PO Box 2040, 3000 CA, Rotterdam, The Netherlands
2 Department of Genetics, King Faisal Specialist Hospital and Research Centre (KFSHRC), Riyadh, 11211, Kingdom of Saudi Arabia

3 KACST-BWH/Harvard Centre of Excellence for Biomedicine, Joint Centers of Excellence Program, King Abdulaziz City for Science and Technology, Riyadh 12354, Saudi Arabia
4 Department of Medical Genetics, King Faisal Specialist Hospital and Research Centre (KFSHRC), Riyadh, 11211, Kingdom of Saudi Arabia
5 Department of Biology, Imam Abdulrahman bin Faisal University, Dammam 34212, Kingdom of Saudi Arabia
6 Genome Research Division, Human Genetics Department, Radboud University Medical Center, Geert Grooteplein Zuid 10, 6525 GA, Nijmegen, The Netherlands
7 Center for Pediatrics and Adolescent Medicine, University Hospital Freiburg, Freiburg University, Faculty of Medicine, Freiburg 79106, Germany
8 Department of Neurosciences, KFSHRC, Riyadh, 11211, Kingdom of Saudi Arabia
9 Department of Pathology and Laboratory Medicine, KFSHRC, Riyadh, 11211, Kingdom of Saudi Arabia
10 Positivo University Medical School, Curitiba, Parana, 81280-330, Brazil
11 Universidade da Região de Joinville, Pós-Graduação em Saúde e Meio Ambiente, Joinville, Santa Catarina, 89219-710, Brazil
12 Núcleo de Assistência Integral ao Paciente Especial, Prefeitura de Joinvile, Joinvile, Santa Catarina, 89202-450, Brazil
13 Department of Medical Genetics and Molecular Medicine, Faculty of Medicine, Mashhad University of Medical Sciences, 9177899191, Mashhad, Iran
14 CENTOGENE GmbH, 18055 Rostock, Germany
15 Medical University of Rostock, 18051 Rostock, Germany
16 Stem Cell and Tissue Re-engineering Program, KFSHRC, Riyadh, 11211, Kingdom of Saudi Arabia
17 Gaziosmanpasa University, School of Medicine, Neurology Dept. Tokat, 8FJH + CW Tokat, Merkez/Tokat, Turkey
18 Koc University, School of Medicine, Suna and Inan Kirac Foundation, NDAL- KUTTAM, Davutpasa cad. No.4, 34010, Zeytinburnu, İstanbul, Turkey
19 Department of Molecular Neuroscience, University College London Institute of Neurology, London WC1N 3BG, UK
20 Department of Molecular and Human Genetics, Baylor College of Medicine, and Baylor Genetics Laboratories, Houston, TX, USA
21 Molecular and Clinical Sciences Institute, St. George's, University of London, Cranmer Terrace, London SW17 0RE, UK
22 Innovative Medical Research Center, Mashhad Branch, Islamic Azad University, 9G58 + 69 Mashhad, Razavi Khorasan Province, Iran
23 Saudi Human Genome Program, King Abdulaziz City for Science and Technology, Riyadh, Kingdom of Saudi Arabia
24 Center for Genomic Medicine, King Faisal Specialist Hospital and Research Center, 11211, Riyadh, Kingdom of Saudi Arabia
25 Department of Molecular Oncology, KFSHRC, Riyadh, 11211, Kingdom of Saudi Arabia
26 Department of Cell Biology, KFSHRC, Riyadh, 11211, Kingdom of Saudi Arabia
27 Division of Biological and Environmental Sciences and Engineering (BESE), Computational Bioscience Research Center (CBRC), King Abdullah University of Science and Technology (KAUST), Thuwal, 23955-6900, Kingdom of Saudi Arabia
28 Centre de Biochimie Structurale, CNRS, INSERM, Université de Montpellier, 34090 Montpellier, France
29 Department of Biostatistics, Epidemiology and Scientific Computing, KFSHRC, Riyadh, 11211, Kingdom of Saudi Arabia
30 Department of Neuromuscular Disorders, UCL Queen Square Institute of Neurology, London, WC1N 3BG, UK

Correspondence to: Namik Kaya
Department of Genetics
NeuroGenetics Unit
King Faisal Specialist Hospital and Research Center
MBC: 03, Riyadh, 11211, Saudi Arabia
E-mail: nkaya@kfshrc.edu.sa

Correspondence may also be addressed to: Tjakko J. van Ham
Department of Clinical Genetics
Erasmus MC University Medical Center
Rotterdam, The Netherlands
E-mail: t.vanham@erasmusmc.nl

Tahsin Stefan Barakat
E-mail: t.barakat@erasmusmc.nl

Miriam Schmidts
Center for Pediatrics and Adolescent Medicine, University Hospital Freiburg, Freiburg University, Faculty of Medicine, Mathildenstrasse 1, Freiburg 79106, Germany
E-mail: miriam.schmidts@uniklinik-freiburg.de

Introduction

Membrane trafficking in eukaryotic cells is critical for protein transport and processing of endocytic cargo for degradation. It is regulated by highly conserved vacuolar protein sorting (VPS) proteins, which were first discovered through genetic screening for yeast mutants exhibiting several classes of distinct trafficking phenotypes (Conibear and Stevens, 1995; Bonangelino *et al.*, 2002). Analogous phenotypes have since been observed in mammalian cells (Huizing *et al.*, 2008) and trafficking defects and VPS protein deficiencies have been linked to numerous human neurological diseases (Supplementary Table 1). For example, a homozygous founder mutation in *VPS11* was found in eight affected individuals from four unrelated Ashkenazi Jewish families who presented with hypomyelination, developmental delay, hypotonia, microcephaly, and seizures (Zhang *et al.*, 2016), while *VPS33A* loss-of-function has been linked to psychomotor retardation, delayed myelination, cerebral calcification, and lysosomal dysfunction (Kondo *et al.*, 2017). However, whether other VPS proteins also have a role in disease remains to be clarified.

VPS proteins frequently function within multi-subunit tethering complexes, the best-documented being the hexameric HOPS (homotypic fusion and vacuole protein sorting) and CORVET (class C core vacuole/endosome tethering) complexes. The HOPS complex is thought to regulate fusion of lysosomes with endo- or autophagosomes and consists of six VPS subunits: VPS39 and VPS41, which are HOPS-specific, as well as VPS11, VPS16, VPS18 and VPS33A, which are also present in the CORVET complex (Bowers and Stevens, 2005). VPS39 and VPS41 interact with RAB7 to specifically target the HOPS complex to late endosomes (Balderhaar and Ungermann, 2013).

Yeast strains with disrupted *VPS41* function exhibit deformities in vacuolar morphology and trans-Golgi trafficking of vacuolar components that can be rescued upon complementation with the wild-type gene (Radisky *et al.*, 1997). As lysosomes in higher eukaryotes are analogous organelles to yeast vacuoles, abnormalities in lysosome-related organelles (LROs)—including lysosomes, melanosomes and phagosomes, among others—are likely to occur in instances of *VPS41* deficiency, for example in vertebrate cells (Delevoye *et al.*, 2019). However, proof of this theory could not be established to date because of early embryonic lethality of the only currently described *Vps41* mouse knockout model preventing further analysis (Aoyama *et al.*, 2012).

Here, we report five unrelated families with nine affected individuals with homozygous missense variants in *VPS41*, presenting with an autosomal recessive, progressive developmental disorder consisting of cerebellar atrophy/hypoplasia, cognitive impairment, motor dysfunction with ataxia and dystonia, and abnormal membrane-bound vesicles, as assessed by electron microscopy in lymphocytes and lymphoblastoid cells.

Materials and methods

Detailed methodology is provided in the Supplementary material.

Human subjects

All probands were investigated by their referring physicians. Most genetic analyses were performed in a diagnostic setting. Legal guardians of affected individuals gave informed consent for genomic investigations and publication of anonymized data. This study was approved by institutional review board of KFSHRC (RAC# 2120022). Exome sequencing was performed as previously described (AlMuhaizea *et al.*, 2020; Perenthaler *et al.*, 2020).

In silico analyses

Functional pathway gene ontology enrichment analyses were performed using Database for Annotation, Visualization and Integrated Discovery (DAVID) (Dennis *et al.*, 2003) and Ingenuity Pathways Analysis (IPA) (QIAGEN Inc.). A right-tailed Fisher's exact test was used to calculate a *P*-value determining the probability that the biological function (or pathway) assigned to that dataset is explained by chance alone. Gene interaction network analysis was performed using IPA. Genes were mapped to their corresponding gene objects in the Ingenuity® Knowledge Base. SwissModel, RaptorX and iTASSER were used to produce homology models. Models were manually inspected and mutations evaluated using PyMOL.

Human embryonic stem cell experiments

VPS41 knockout embryonic stem cells (ESCs) were generated by clustered regularly interspaced short palindromic repeats (CRISPR)-Cas9 mutagenesis, as previously described (Barakat *et al.*, 2018; Perenthaler *et al.*, 2020). ESCs were used in rescue experiments in which wild-type or mutant VPS41 was expressed transiently. Full experimental details are provided in the Supplementary material.

CRISPR/Cas9 zebrafish mutagenesis

CRISPR/Cas9 mutagenesis was performed largely as previously described using guide RNA (gRNA) targeting exon 4 of *vps41*. Cas9 nuclease was synthesized (Kuil *et al.*, 2019) and co-injected with gRNAs into fertilized zebrafish oocytes. Indel efficiency and frequency were determined using Sanger sequencing.

LysoTracker^TM staining

For LysoTracker^TM staining, carried out as previously described (Kuil *et al.*, 2019), zebrafish larvae were incubated in the dark at 2°C for 40 min in 1.5 ml tubes with 100 µl LysoTracker^TM Red DND-99 (ThermoFisher) diluted to a final concentration of 10 µM in E3 media containing 200 µM PTU. Medium was replaced with fresh E3-PTU and incubated 20 min before imaging.

In vivo imaging and image analysis

Larvae were anaesthetized using tricaine (0.016%) prior to being mounted in 1.8% low melting point agarose (Kuil *et al.*, 2019). *In vivo* fluorescence imaging used a Leica SP5 intravital confocal microscope with a 20× water-dipping objective (Leica Plan-Apochromat, NA = 1.0). Images were analysed using ImageJ software (Schindelin *et al.*, 2012).

Optokinetic response assay

Zebrafish embryos [5 days post-fertilization (dpf)] were positioned in 6% methylcellulose/1× E3 within clear plastic wells and placed on a platform surrounded by a motorized drum (20 rpm) lined with black and white stripes of defined spatial frequencies on interchangeable inserts. Embryos were assessed for 1 min per trial, with trials consisting of assessment in both clockwise and counterclockwise directions with inserts achieving either 0.06 or 0.10 cycles per degree. Infrared monitoring and a custom program written by Dr Frank Schaeffel (University of Tübingen) were used to monitor and measure eye movement/position.

Statistical analyses

For continuous variables, data are reported either as individual values with the median and standard error of the mean (SEM) indicated or as box and whisker plots indicating the interquartile range (IQR) and median, minimum, and maximum values of the range. Categorical variables are summarized as percentages. Continuous variables were compared by Student's *t*-test (or Mann-Whitney U-test) or one-way ANOVA as applicable, while the categorical variables are compared by Fisher's exact test. Statistical analyses were conducted using GraphPad Prism 6.00 (La Jolla, California, USA) and PARTEK Genomics Suite (Partek Inc., St. Lois, MO, USA). The statistical level of significance was set at $P < 0.05$.

Data availability

The data that support the findings of this study are available from the corresponding authors, upon reasonable request, with the exception of primary patient sequencing data, which cannot be made available due to patient consent.

Results

Clinical phenotype and genetic investigations

Affected individuals were born after uneventful pregnancies and presented in most cases early in life with developmental delay (Fig. 1, Table 1, Supplementary Figs 1–5 and Supplementary Table 2). Various degrees of ataxia, hypotonia, and dystonia were present in all affected individuals, preventing independent ambulation. Likewise, nystagmus was commonly described. In addition, all affected individuals displayed intellectual disability and speech delay. Two siblings further presented with therapy-resistant epilepsy. No major dysmorphic features were found. In two individuals, retinal pigment alterations were noticed. Brain MRI revealed mild cerebellar atrophy and vermian atrophy without other major structural abnormalities in most affected individuals while in one case (Subject 9) bilateral hyperintensities at the nucleus caudatus area were noted (Fig. 1C and Supplementary Fig. 5). No hearing or vision problems were noted and in cases where nerve conduction studies were performed, these were normal. Transmission electron microscopy (TEM) on peripheral blood lymphocytes from Subject 2 and lymphoblastoid cells from Subject 3 revealed more multilayered vesicles compared to control cells (Supplementary Fig. 6).

Exome sequencing did not identify variants in known disease genes but revealed homozygous missense variants in *VPS41* (GenBank: NM_014396) that fully segregated with the phenotype in families where segregation analysis was performed (Fig. 1A and Supplementary Figs 2–5). No other likely pathogenic variants were identified. Other than c.853T>C (p.Ser285Pro), which was found twice in a heterozygous state in gnomAD (minor allele frequency: 0.000007), the encountered variants [c.1898G>C (p.Arg633Pro), c.2372G>T (p.Cys791Phe), and c.38A>G (p.Glu13Gly)] have not previously been reported in publicly available genome databases (Fig. 1D). All variants were family-specific except for c.853T>C (p.Ser285Pro), which was encountered in two different families from Saudi Arabia. All missense variants occur in evolutionarily conserved amino acid positions that *in silico* modelling suggests are likely to disturb protein structure (Fig. 1D and E and Supplementary Fig. 7A and B).

In silico analysis predicts reduced VPS41 function in affected individuals

Protein modelling showed that VPS41 contains an acidic N-terminal extension (residues 1–29), a WD40 β-propeller domain (residues 30–361), a central superhelical structure composed of clathrin heavy-chain repeats (CHCR; residues 362–81) and a C-terminal RING (really interesting new gene) zinc finger (787–852) (Fig. 1D and E). Glu13Gly
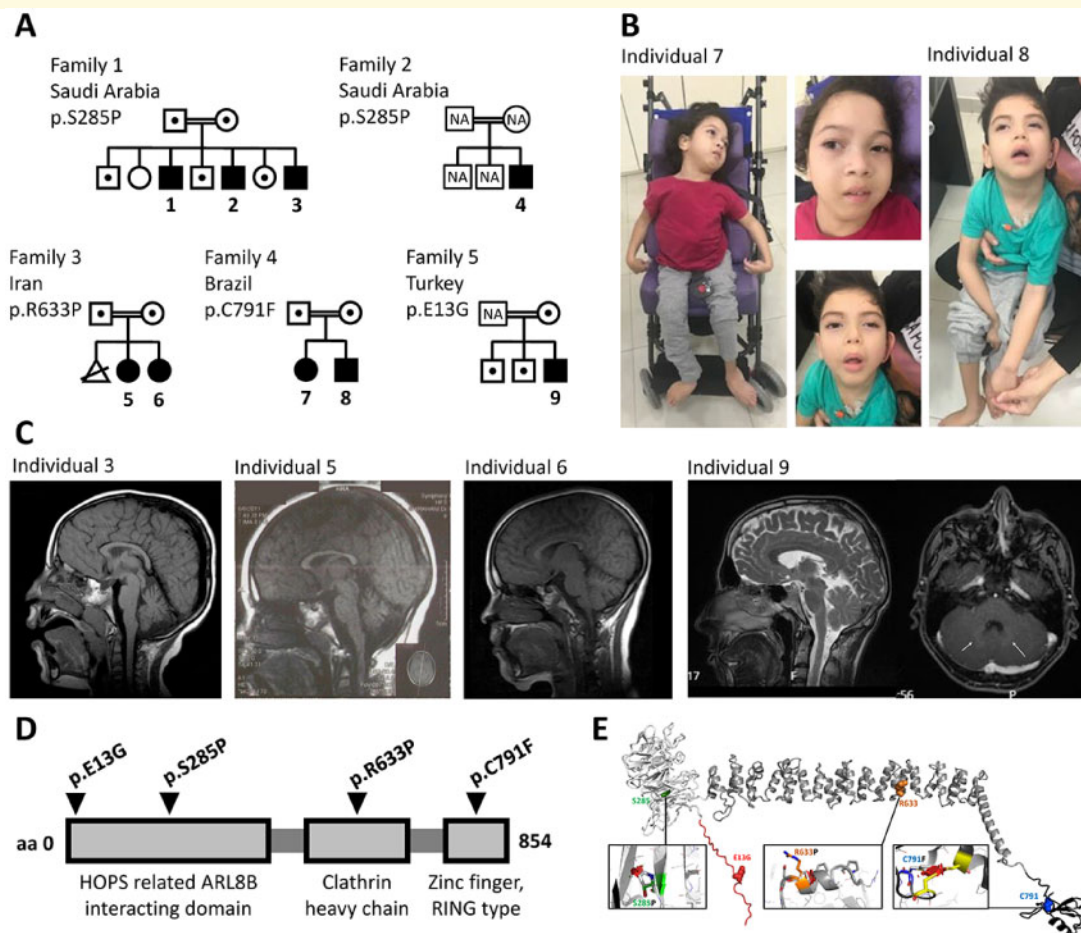
Figure 1 Bi-allelic variants in *VPS41* lead to a progressive developmental disorder with cerebellar dysfunction. (**A**) Pedigrees of Families 1–5 with affected Subjects 1–9 (closed symbols), with carriers indicated by dots. (**B**) Frontal facial and full body photographs of Subjects 7 (female) and 8 (male) in a sitting position; both children were wheelchair-bound. Individuals present with hypotonic face, slightly low-set ears, long eyelashes, full cheeks, small, open mouth with full lips. Full body images illustrate failure to thrive, marked hypotonia in Subject 8, spastic thoracic deformity, and flexion contractures in the upper limbs of the Subject 7. (**C**) Brain MRI of affected Subjects 3, 5, 6 and 9, showing midline vermian atrophy (Subject 3), mild cerebellar vermis hypoplasia/atrophy (Subject 5), milder (compared to the sibling Subject 5) cerebellar vermis hypoplasia/atrophy (Subject 6) and no overt cerebellar volume reduction (first image) but bilateral hyperintensities in the nucleus caudatus area (arrows, second image) (Subject 9). (**D**) Schematic overview of the VPS41 protein with identified variants indicated. (**E**) Structural protein modelling showing that VPS41 contains an acidic N-terminal extension (residues 1–29, red), a WD40 β-propeller domain (residues 30–361, white), a central superhelix structure composed of clathrin heavy-chain repeats (CHCR; residues 362–781, grey) and a C-terminal RING zinc-finger (787–852, black). The complete structure is shown in the centre as a ribbon drawing, with the mutated residues highlighted as coloured sphere models. The *insets* show the structural context of each mutation, except for E13G, which is located in a flexible region. The other *insets* show the original residue as a stick model, coloured as in the overview. The mutated residue is shown superimposed as a white stick model. Size and orientation of the red discs show the extent and direction of steric clashes.

attenuates the acidic charge of the N-terminal extension. Glu-rich acidic regions are frequently used for protein localization and ligand recognition (Uversky, 2013) and the mutation might abrogate such functions. Ser285Pro affects the WD40 domain. Ser285 is part of a buried β-strand and a proline in this position would disrupt this secondary structure and decrease shape complementarity within the densely packed protein core. Because of this disruptive effect on the WD40 domain, Ser285Pro might affect ARL8B binding (Khatter *et al.*, 2015). The interaction of VPS41 with ARL8B through its effector SKIP (SifA and kinesin-

interacting protein) contributes to lysosomal localization and trafficking and degradation of EGFR (Khatter *et al.*, 2015). Interestingly, when Arl8b is silenced, lysosomal cargo delivery is impaired (Khatter *et al.*, 2015). The Arg633Pro mutation found within the CHCR distorts the α-helix because the rigidity of proline and its inability to donate a hydrogen bond lead to strong kinks in helices. Finally, residue 791 represents the first cysteine of the zinc finger/RING-type domain and its mutation to Phe is expected to abolish zinc binding and would introduce steric clashes (Matthews and Sunde, 2002). Thus, each of the identified variants is

Table 1 Clinical details of the affected individuals

Individual	Family 1			Family 2	Family 3		Family 4		Family 5
	1	2	3	4	5	6	7	8	9
Variant; cDNA	c.853T>C			c.853T>C	c.1898G>C		c.2372G>T		c.38A>G
Variant; protein	p.Ser285Pro			p.Ser285Pro	p.Arg633Pro		p.Cys791Phe		p.Glu13Gly
Current age, years	27	22	13	2	15	11	7	11	28
Ethnicity	Arab (Saudi)			Arab (Saudi)	Asian (Iran)		Caucasian (Brazil)		Asian (Turkish)
Gender	Male	Male	Male	Male	Female	Female	Male	Female	Male
Early motor development	Delayed	Delayed	Delayed	Delayed	Delayed		Delayed, neuroregression	Delayed, neuroregression	Delayed
Myopathic face	Yes	Yes	Yes	No	Yes	No	No	No	No
Seizures	No	No	No	No	No	No	Yes	Yes	No
Cognitive impairment	Yes	Yes	Yes	Yes	Yes	Yes	Neurological regression	Neurological regression	Mild
Smooth pursuit eye movement	Abnormal	Abnormal	No	NR	NR	NR	Yes	Yes	No
Retinal examination	Normal	Normal	Normal	NR	NR	NR	Salt and pepper retinal lesion		Normal
Cerebellar ataxia	Yes	Yes	Yes	Yes	Yes	Yes	NA	NA	Yes
Dysarthria	Yes	Yes	Yes	Absent speech	Yes	Yes	Absent speech	Absent speech	Yes
Nystagmus	Horizontal on lateral gaze	Horizontal on lateral gaze	No	NR	Yes	Yes	Only when seizures occur	No	Yes
Tone	Hypotonic	Hypotonic	Hypotonic	Hypotonic	Axial tone reduced	Axial tone reduced	Generalized hypotonia, wheelchaired	Generalized hypotonia, wheelchaired	Spastic for the lower extremities
MRI	Midline vermian atrophy, no iron deposition	Midline vermian atrophy, no iron deposition	Midline vermian atrophy, no iron deposition	NA	Mild vermis hypoplasia or atrophy	Mild vermis hypoplasia or atrophy	Mild atrophy of cerebellar vermis, hemispheres and the middle cerebellar peduncles	Atrophy of the corpus callosum and cerebellar hemispheres and brainstem; abnormal iron deposition in the globus pallidus and substantia nigra; supratentorial ventricular dilation	Atrophy of cerebrum and mild cerebellar atrophy; Hyperintense lesions in T_2 in the cerebellar hemispheres, nucleus dentatus, supratentorial white matter lesions

DTR = deep tendon reflex; NA = not applicable; NR = not reported.

predicted to affect protein domains implicated in mediating ligand interactions, possibly leading to an impact on VPS41 function and stability. The level of weakening or disruption of these interactions possibly explains the diverse patient specific differences (Fig. 1E, Table 1 and Supplementary Table 2).

VPS41 is moderately expressed in the cerebral cortex and cerebellum (Supplementary Fig. 8A), but is expressed highly in Purkinje cells (Supplementary Fig. 8B). Since co-expressed genes are considered more likely to be functionally related and may provide clues about gene function and regulation (Stuart *et al.*, 2003; van Dam *et al.*, 2015), we searched for genes that are co-regulated with *VPS41* in over 4000 human RNASeq data (van Dam *et al.*, 2015; Al-Harazi *et al.*, 2019). We identified 105 genes (correlation coefficient ⩾ 0.4), of which almost 80%, like *VPS41*, are expressed in the nervous system (Supplementary Table 3). Functional enrichment and pathway analyses of *VPS41* co-expressed genes revealed significant enrichment for terms associated with nervous system development and function, vesicle-mediated transport, cellular component organization, phagosome maturation and autophagy pathways (*VPS39*, *VPS41* and *PIK3C3*) (all *P*-values < 0.01) (Supplementary Fig. 9 and Supplementary Tables 4–6).

VPS41 variants show functional defects in human embryonic stem cells

To functionally test VPS41 variants in a cellular model, we generated human ESCs knock-out (KO) for VPS41 by CRISPR-Cas9 engineering (Barakat *et al.*, 2018; Perenthaler *et al.*, 2020). A clone was obtained harbouring a homozygous 1 bp insertion (chr7:38908803_38908804insT), leading to a frameshift and premature stop codon (c.110_111insA, N37Kfs*5), resulting in the full absence of all VPS41 as assessed by immunoblotting (Supplementary Fig. 10A–C). VPS41 KO did not alter ESC growth characteristics but resulted in minor flattened morphology compared to parental wild-type ESCs (Supplementary Fig. 10D). Previous work showed that the transcription factor TFE3 can be cytoplasmic or nuclear, depending on its phosphorylation state, and that this is regulated by mTORC1 signalling and lysosomes (Yang *et al.*, 2018; Shin and Zoncu, 2020). In agreement with lysosomal dysfunction (Villegas *et al.*, 2019), the absence of VPS41 resulted in solely nuclear TFE3 localization (Fig. 2A). VPS41 KO cells showed upregulation of the lysosomal protein LAMP2 (Fig. 2C, D and Supplementary Fig. 10E), likely due to nuclear TFE3 localization (Fan *et al.*, 2018). Thus, the absence of VPS41 provided two clear phenotypical differences between wild-type and VPS41 KO ESCs and we used the cellular phenotype of this VPS41 KO background to assess the functionality of wild-type and mutant VPS41 proteins in rescue experiments. We used the expression of V5-VPS41-T2A-GFP fusions, allowing the tracking of transfected cells at the population

and single cell level. Fluorescence-activated cell sorting (FACS) analysis 48 h after transient transfection showed a significant reduction in the percentage (Fig. 2E) and intensity (Supplementary Fig. 10F) of GFP + cells for the Arg633Pro and Cys791Phe variants, whereas transfection efficiency for a spiked-in mCherry control was similar amongst all transfections (Supplementary Fig. 10G). In agreement, immunoblotting confirmed reduced protein expression of these both mutants, as well as a slightly reduced expression of Ser285Pro (Fig. 2C and D). This indicates that the variants encountered result in reduced RNA or protein expression and possibly stability. Whereas transfection of wild-type VPS41 resulted in downregulation of LAMP2 in transfected KO ESCs, expression of Ser285Pro, Cys791Phe, and to a lesser extent Arg633Pro, failed to downregulate LAMP2 at a population level (Fig. 2D). We then moved to single cells and evaluated the cellular distribution of TFE3. Upon transient transfection of wild-type VPS41, cytoplasmic localization of TFE3 was restored in GFP + cells (Fig. 2A and B). In contrast, transient transfection of Glu13Gly resulted in a significantly reduced rescue of the TFE3 cytoplasmic localization in GFP + cells, indicating a reduced functionality of this mutant despite normal protein expression (Fig. 2A and B). TFE3 relocalization was similar for Ser285Pro, Arg633Pro, and Cys791Phe in GFP + cells, indicating that if sufficient overexpression can be achieved, these mutants can promote TFE3 relocalization. Together, these data further support our *in silico* analysis, providing functional evidence that the encountered variants affect VPS41 protein expression levels and result in measurably reduced VPS41 function in human cells.

Zebrafish disease modelling recapitulates key clinical findings

To investigate the neurological effects of VPS41 loss *in vivo*, we mutated the single *vps41* homologue in zebrafish, which shares 82% amino acid identity with the human protein, by injection of CRISPR/Cas9 and gRNA ribonucleoprotein complexes into oocytes (Supplementary Fig. 11). CRISPR-mediated mutants (crispants) generated in this way have been shown to exhibit highly efficient mutagenesis, often achieving complete loss of the wild-type target sequence, and can reliably phenocopy existing loss-of-function mutants and thus facilitate rapid and reliable investigations in F0 embryos (Shah *et al.*, 2015; Kuil *et al.*, 2019). Zebrafish *vps41* crispants, having a *vps41* disruption efficiency between 60 and 90%, had normal general morphology in the first 3 days but displayed a severe lack of pigmented melanocytes when compared to control gRNA-injected oocytes (Fig. 3A). Pigmentation defects were partially corrected by injection of wild-type *vps41* mRNA at the 1–2-cell stage (Supplementary Fig. 11). After 5 days, 100% of *vps41* crispants showed a lack of swim bladder inflation—ultimately resulting in a loss of viability—as well as decreased body length and reduced pigmentation both throughout the body and in the retina (Fig. 3A–C). These specific pigmentation phenotypes are
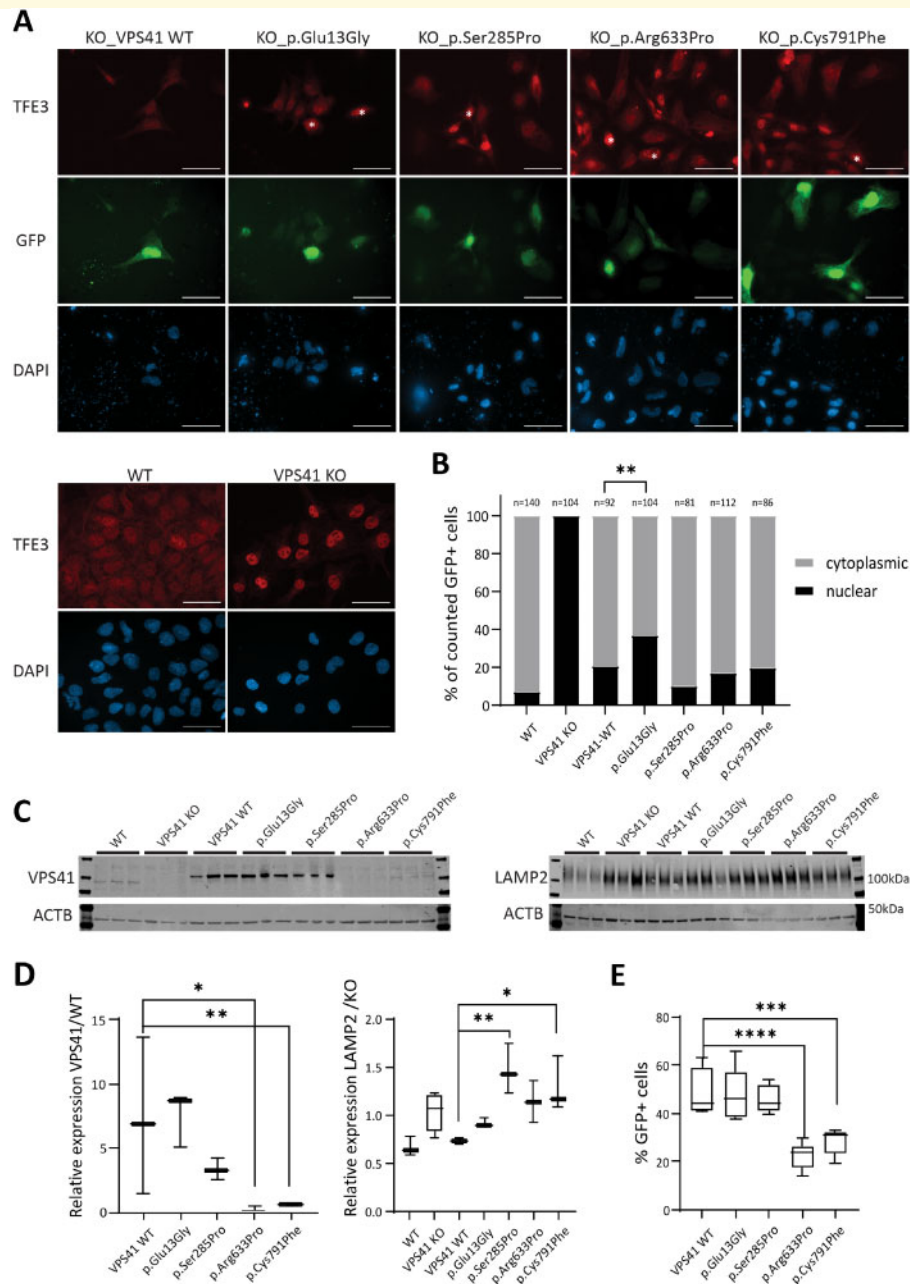
Figure 2 *VPS41* variants contribute to impaired lysosomal functions *in vitro*. (**A**) Immunocytochemistry assessing TFE3 in rescue experiments using transient expression of wild-type (WT) and mutant VPS41-t2a-GFP in VPS41 KO ESC. Transfected cells are marked by GFP and GFP + cells showing no TFE3 relocalization to the cytoplasm are marked with white asterisks. Nuclei are counterstained with DAPI. Scale bars = 50 μm. (**B**) Quantification of **A** counting a minimum of 80 GFP + cells from three replicates. ***P = 0.0001, binomial test (expected distribution based on relocalization upon transfection with the wild-type construct). (**C**) Western blotting detecting VPS41 (endogenous VPS41 99 kDa, V5-tag-VPS41 105 kDa, input 30 μg) and LAMP2 (100–120 kDa, input 20 μg), in wild-type and VPS41 KO ESCs and VPS41 KO ESCs transiently rescued with wild-type or mutant VPS41. (**D**) Quantification of **C**, *P < 0.05; **P < 0.01; ***P < 0.001 one-way ANOVA, multiple comparison test of mutant constructs to the wild-type. (**E**) Percentage of GFP + cells upon transient transfections of VPS41-KO cells with VPS41-GFP plasmid spiked with mCherry, expressing wild-type or mutant VPS41. ***P = 0.0006, ****P < 0.0001, one-way ANOVA, multiple comparison test of mutant constructs to the wild-type; >17 000 cells were analysed per sample.

consistent with observations of loss-of-function of other HOPS components *vps33a/Vps33a* in mice and *vps11*, *vps18* and *vps39* in zebrafish (Thomas *et al.*, 2011; Zhen and Li, 2015; Berg *et al.*, 2016), while swim bladder defects

were also noted in all three zebrafish mutants. Deficiencies in surfactant production or distribution during swim bladder development are believed to contribute to an inability to properly inflate (Chen *et al.*, 2018). Together, these data
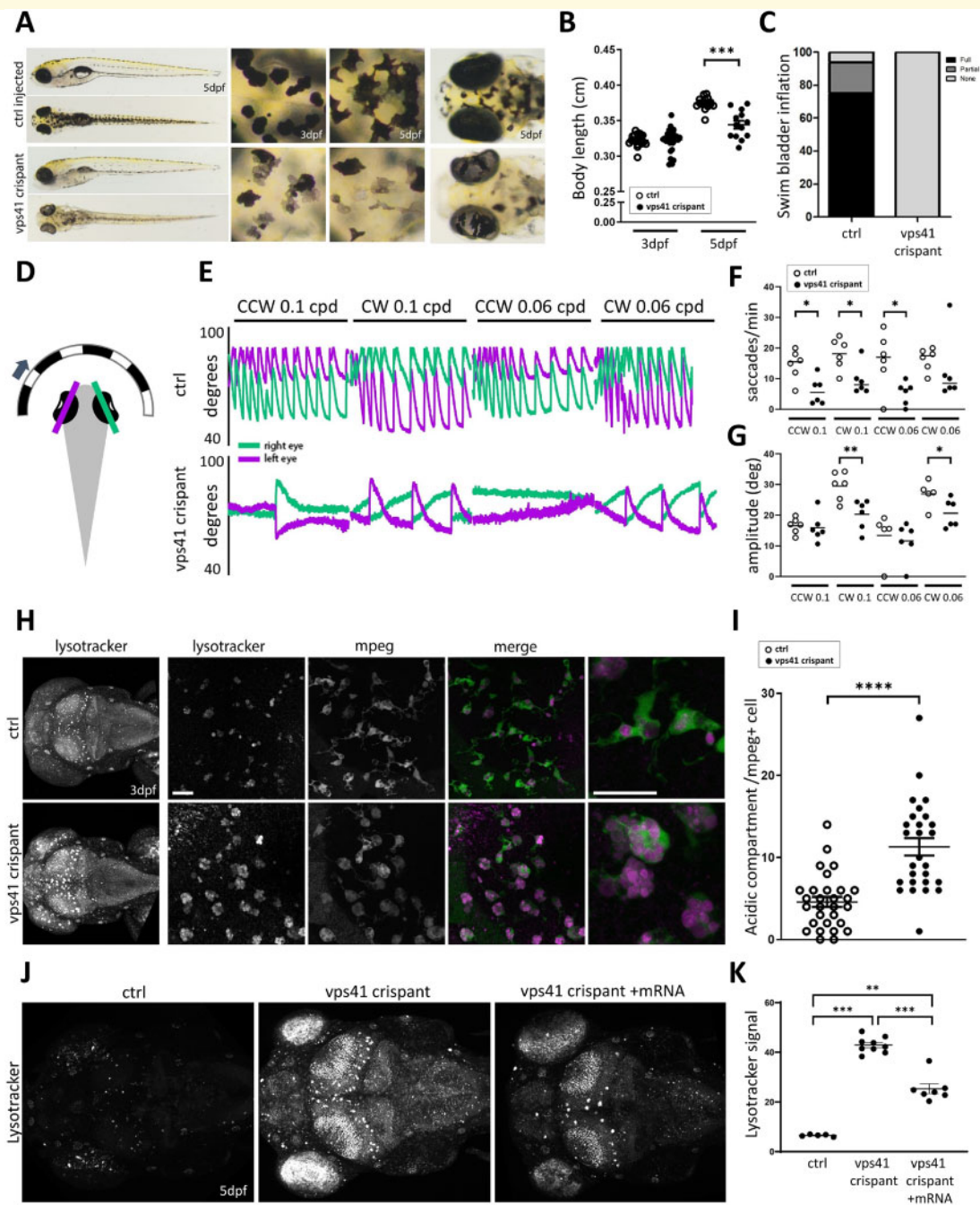
Figure 3 VPS41 disease modelling in zebrafish recapitulates lysosomal abnormalities and indicates microglial and cerebellar dysfunction. (**A**) Gross morphology of *vps41* crispant versus control embryos at 5 dpf. Magnified views of the skin and eyes show abnormal melanocyte morphology and reduced pigmentation in both the skin melanocytes and retinal pigment epithelium. (**B**) Measurements of body length at 3 and 5 dpf, suggesting a reduced growth rate in *vps41* crispants versus controls (*n* = 15 each). (**C**) At 5 dpf, swim bladders were not visible in any of the *vps41* crispant embryos, while being fully developed by this time in the majority of controls (*n* = 50). (**D**) Schematic of the OKR experiment, indicating the eye angles measured. (**E**) Representative OKR traces for *vps41* crispant and control embryos under four different conditions. (**F**) Quantification of saccades produced in response to visual stimuli (*n* = 6 for each condition). (**G**) Average saccade amplitude per trial, taken from left eye traces (*n* = 6 for each condition). (**H**) LysoTracker™ staining of 3 dpf embryos, revealing increased acidification of *vps41* crispant brains that is largely concentrated within Mpeg1 + cell (microglia) compartments. Scale bars = 20 µm. (**I**) Quantification of acidic compartments within microglia in the brain at 3 dpf (6–8 cells counted per embryo, *n* = 4 embryos each). (**J**) Compared to control injected embryos at 5 dpf, *vps41* crispants show a remarkably increased level of acidity across the entire brain, detected using LysoTracker™, that is significantly reduced when embryos are additionally injected with wild-type *vps41* mRNA at the 1–2 cell stage. (**K**) Quantification of the LysoTracker™ signal intensity across the whole brain of 5 dpf control, *vps41* and *vps41* + mRNA-injected embryos (*n* = 5 controls, *n* = 9 *vps41*, and *n* = 7 *vps41* + mRNA). Data-points in **B**, **F**, **G** and **I** are individual measurements (circles) and mean (bars) and error bars indicate SEM. CW = clockwise; CCW = counterclockwise; cpd = cycles per degree; dpf = days post-fertilization. $*P < 0.05$; $**P < 0.01$; $***P < 0.001$; $****P < 0.0001$.

further support a role for Vps41 and the HOPS complex in the development and function of LROs, including both melanosomes (the pigment-producing organelles within melanocytes and the retinal pigment epithelium) and the surfactant-producing organelles involved in the teleost surfactant production system (Chen *et al.*, 2018; Delevoye *et al.*, 2019).

Abnormal eye movements are associated with cerebellar injury and can be diagnostic of ataxia (Cogan *et al.*, 1982). Thus, we analysed the optokinetic response (OKR) of *vps41*-mutated zebrafish larvae, using a well-established zebrafish assay for cerebellar dysfunction (Namikawa *et al.*, 2019). In contrast to control injected larvae, which demonstrated normal responses to visual stimuli, *vps41* crispants showed a dramatically reduced response and, when present, saccades had both reduced amplitude and frequency (Fig. 3D–G), indicating defects in eye movement control and suggesting cerebellar dysfunction. Spontaneous eye movements in the absence of stimulation were observed, removing the possibility that crispants were simply unable to move their eyes. The underlying mechanisms of reduced visual performance seen in *vps41* crispants remain unclear. Nevertheless, data from both *vps11* and *vps39* mutant zebrafish indicate that ineffective digestion of material phagocytosed by the retinal pigment epithelium could contribute by hindering proper development and function of photoreceptor cells, further pointing to a defect in LRO function (Schonthaler *et al.*, 2007; Thomas *et al.*, 2011).

While no differences were seen in the gross morphology or size of *vps41* crispant brains (Supplementary Fig. 11C), we sought to further investigate potential underlying neurological abnormalities that could help understand the progressive neurodevelopmental phenotypes seen in human disease. During early neurodevelopment microglia are highly endocytic and phagocytic, functions that rely heavily on efficient membrane trafficking and LRO function, the dysfunction of which is readily observed in zebrafish larvae (Berg *et al.*, 2016; Kuil *et al.*, 2019). Early defects in microglial function have been linked to a wide range of neurological diseases, including lysosomal storage diseases, where lysosomal dysfunction in microglia has been implicated as a primary driver (Kuil *et al.*, 2019). Thus, to assess whether microglial dysfunction may play a role in VPS41 variant-driven pathology, we used neutral red staining to observe microglia during development of *vps41* crispants and control larvae (Supplementary Fig. 11B). This revealed that *vps41*-deficient microglia have distinct morphological abnormalities suggestive of larger, or possibly more numerous, lysosomal compartments compared to microglia from control larvae. To more carefully dissect this phenotype, we sought to visualize lysosomes *in vivo* in the developing brain using LysoTracker™ in zebrafish where microglia were transgenically tagged with green fluorescent protein (GFP). Confocal imaging revealed that *vps41* deficiency resulted in a dramatic increase in LysoTracker™ signal throughout the entire brain, in addition to highly amoeboid, swollen microglia with large, supernumerary acidic compartments in contrast to those in control injected zebrafish (Fig. 3H and I).

Importantly, LysoTracker™ signal in the brain was significantly abrogated by the injection of wild-type zebrafish *vps41* mRNA into crispant oocytes at the 1–2-cell stage (Fig. 3J and K), again supporting the specificity of our observations and utility of this model for the study of *vps41* function. Together, these data further support a role for lysosomal dysfunction upon *vps41* disruption and, in parallel with observations of macrophage defects seen in *vps39* mutant zebrafish (Schonthaler *et al.*, 2007), suggest disruption of microglial function. However, while the largest LysoTracker + compartments both in crispants and controls appeared within *mpeg* + cells, it is important to note that a substantial increase in LysoTracker + compartments inside cells other than microglia was also observed only in *vps41* crispants. This supports a more global LRO defect that likely impacts neural progenitors as well, contributing to developmentally seeded neurological defects that are likely further compounded by microglial dysfunction.

Discussion

Here we establish that *VPS41* bi-allelic mutations cause cerebellar ataxia. As the identified variants fail to completely rescue the lysosomal dysfunction seen in VPS41 KO ESCs, and VPS41 deficiency causes lysosomal abnormalities in multiple brain cell types in the developing zebrafish brain, it is possible that membrane trafficking defects in neurons underlie cerebellar atrophy. Additionally, gene network analysis suggests that VPS41 dysfunction may disrupt a number of signalling pathways linked to neuronal development and maintenance of brain function (Supplementary Fig. 9 and Supplementary Tables 4–6). Nearly all spinocerebellar ataxias have been characterized by Purkinje cell deterioration and cerebellar atrophy (Huang and Verbeek, 2018). A scenario of reduced viability of Purkinje cells is also plausible for VPS41-related ataxia and may help explain cerebellar atrophy. Although we did not detect clear differences directly in zebrafish Purkinje cells during the early development of *vps41* crispants (Supplementary Fig. 11D), cellular dysfunction is supported by our OKR results and may precede visible deterioration. However, we did observe distinct lysosomal accumulation and abnormalities at a very early stage in microglia. As lysosomal accumulation in microglia inhibits their function and thus is detrimental to brain development and function, combined with the understanding that a loss of microglia has been shown to cause a spectrum of brain abnormalities, including cerebellar hypoplasia (Oosterhof *et al.*, 2019; Burns *et al.*, 2020), further investigation of the role of microglia in the disease pathogenesis is warranted.

It is interesting to note the overlap of some phenotypes observed in models of VPS loss-of-function, yet ours is the first report to explicitly link variants in a HOPS-specific *VPS* gene to human brain disease. Intriguingly, many of the existing *Vps/vps* mutant animal models were identified in genetic screens for pigmentation defects and have been proposed to model Hermansky-Pudlak syndrome (HPS), a disorder

typified by albinism and bleeding, but typically no neurological abnormalities. Mutations associated with HPS include mutations in genes involved in LRO biogenesis, though to date no *VPS* mutations have been linked to this disease in humans (Merideth *et al.*, 2020). This suggests that while LRO dysfunction contributes to familiar phenotypes across a spectrum of human diseases, *VPS* (and specifically HOPS) mutations diverge from other LRO-associated diseases as they appear to more prominently affect the nervous system. VPS mutant animal models may therefore require reassessment and possible reclassification as models of cerebellar dysfunction.

Together, our work provides evidence that genetic defects in *VPS41*, and thus the HOPS complex, result in dysregulated neurodevelopment in vertebrates, with a predominant ataxia phenotype, driven at least partially through LRO abnormalities. We suggest that screening for *VPS41* variants, and perhaps other HOPS members, should therefore be considered among cases of unsolved autosomal recessive ataxia. Our work adds to the increasing knowledge on autosomal recessive cerebellar ataxias by providing evidence that genetic defects in the HOPS-specific subunit *VPS41* lead to abnormalities in lysosome-related organelles in multiple cell types, including microglia. This contributes to disturbed neurodevelopment and ataxia, though further studies are needed to clearly dissect the underlying mechanisms of these connections.

Acknowledgements

Funding

Competing interests

Supplementary material

Supplementary material is available at *Brain* online.

References

Al-Harazi O, El Allali A, Colak D. Biomolecular databases and subnetwork identification approaches of interest to big data community: an expert review. OMICS 2019; 23: 138–51.

AlMuhaizea M, AlMass R, AlHargan A, AlBader A, Medico Salsench E, Howaidi J, et al. Truncating mutations in YIF1B cause a progressive encephalopathy with various degrees of mixed movement disorder, microcephaly, and epilepsy. Acta Neuropathol 2020; 139: 791–4.

Aoyama M, Sun-Wada GH, Yamamoto A, Yamamoto M, Hamada H, Wada Y. Spatial restriction of bone morphogenetic protein signaling in mouse gastrula through the mVam2-dependent endocytic pathway. Dev Cell 2012; 22: 1163–75.

Balderhaar HJ, Ungermann C. CORVET and HOPS tethering complexes—coordinators of endosome and lysosome fusion. J Cell Sci 2013; 126: 1307–16.

Barakat TS, Halbritter F, Zhang M, Rendeiro AF, Perenthaler E, Bock C, et al. Functional dissection of the enhancer repertoire in human embryonic stem cells. Cell Stem Cell 2018; 23: 276–88 e8.

Berg RD, Levitte S, O'Sullivan MP, O'Leary SM, Cambier CJ, Cameron J, et al. Lysosomal disorders drive susceptibility to tuberculosis by compromising macrophage migration. Cell 2016; 165: 139–52.

Bonangelino CJ, Chavez EM, Bonifacino JS. Genomic screen for vacuolar protein sorting genes in *Saccharomyces cerevisiae*. Mol Biol Cell 2002; 13: 2486–501.

Bowers K, Stevens TH. Protein transport from the late Golgi to the vacuole in the yeast Saccharomyces cerevisiae. Biochim et Biophys Acta 2005; 1744: 438–54.

Burns JC, Cotleur B, Walther DM, Bajrami B, Rubino SJ, Wei R, et al. Differential accumulation of storage bodies with aging defines discrete subsets of microglia in the healthy brain. eLife 2020; 9:

Chen T, Song G, Yang H, Mao L, Cui Z, Huang K. Development of the swimbladder surfactant system and biogenesis of lysosome-related organelles is regulated by BLOS1 in Zebrafish. Genetics 2018; 208: 1131–46.

Cogan DG, Chu FC, Reingold DB. Ocular signs of cerebellar disease. Arch Ophthalmol 1982; 100: 755–60.

Conibear E, Stevens TH. Vacuolar biogenesis in yeast: sorting out the sorting proteins. Cell 1995; 83: 513–6.

Delevoye C, Marks MS, Raposo G. Lysosome-related organelles as functional adaptations of the endolysosomal system. Curr Opin Cell Biol 2019; 59: 147–58.

Dennis G Jr, Sherman BT, Hosack DA, Yang J, Gao W, Lane HC, et al. DAVID: database for Annotation. Genome Biol 2003; 4: P3.

Fan T, Pi H, Li M, Ren Z, He Z, Zhu F, et al. Inhibiting MT2-TFE3-dependent autophagy enhances melatonin-induced apoptosis in tongue squamous cell carcinoma. J Pineal Res 2018; 64: e12457.

Huang M, Verbeek DS. Why do so many genetic insults lead to Purkinje Cell degeneration and spinocerebellar ataxia? Neurosci Lett 2018; 688: 49–57.

Huizing M, Helip-Wooley A, Westbroek W, Gunay-Aygun M, Gahl WA. Disorders of lysosome-related organelle biogenesis: clinical and molecular genetics. Annu Rev Genom Hum Genet 2008; 9: 359–86.

Khatter D, Raina VB, Dwivedi D, Sindhwani A, Bahl S, Sharma M. The small GTPase Arl8b regulates assembly of the mammalian HOPS complex on lysosomes. J Cell Sci 2015; 128: 1746–61.

Kondo H, Maksimova N, Otomo T, Kato H, Imai A, Asano Y, et al. Mutation in VPS33A affects metabolism of glycosaminoglycans: a new type of mucopolysaccharidosis with severe systemic symptoms. Hum Mol Genet 2017; 26: 173–83.

Kuil LE, López Martí A, Carreras Mascaro A, Bosch JC, Berg P, Linde HC, et al. Hexb enzyme deficiency leads to lysosomal abnormalities in radial glia and microglia in zebrafish brain development. Glia 2019; 67: 1705–18.

Matthews JM, Sunde M. Zinc fingers–folds for many occasions. IUBMB Life 2002; 54: 351–5.

Merideth MA, Introne WJ, Wang JA, O'Brien KJ, Huizing M, Gochuico BR. Genetic variants associated with Hermansky-Pudlak syndrome. Platelets 2020; 31: 544.

Namikawa K, Dorigo A, Zagrebelsky M, Russo G, Kirmann T, Fahr W, et al. Modeling neurodegenerative spinocerebellar ataxia type 13 in Zebrafish using a purkinje neuron specific tunable coexpression system. J Neurosci 2019; 39: 3948–69.

Oosterhof N, Chang IJ, Karimiani EG, Kuil LE, Jensen DM, Daza R, et al. Homozygous mutations in CSF1R cause a pediatric-onset leukoencephalopathy and can result in congenital absence of microglia. Am J Hum Genet 2019; 104: 936–47.

Perenthaler E, Nikoncuk A, Yousefi S, Berdowski WM, Alsagob M, Capo I, et al. Loss of UGP2 in brain leads to a severe epileptic encephalopathy, emphasizing that bi-allelic isoform-specific start-loss mutations of essential genes can cause genetic diseases. Acta Neuropathol 2020; 139: 415–42.

Radisky DC, Snyder WB, Emr SD, Kaplan J. Characterization of VPS41, a gene required for vacuolar trafficking and high-affinity iron transport in yeast. Proc Natl Acad Sci USA 1997; 94: 5662–6.

Schindelin J, Arganda-Carreras I, Frise E, Kaynig V, Longair M, Pietzsch T, et al. Fiji: an open-source platform for biological-image analysis. Nat Methods 2012; 9: 676–82.

Schonthaler HB, Fleisch VC, Biehlmaier O, Makhankov Y, Rinner O, Bahadori R, et al. The zebrafish mutant lbk/vam6 resembles human multisystemic disorders caused by aberrant trafficking of endosomal vesicles. Development 2007; 135: 387–99.

Shah AN, Davey CF, Whitebirch AC, Miller AC, Moens CB. Rapid reverse genetic screening using CRISPR in zebrafish. Nat Methods 2015; 12: 535–40.

Shin HR, Zoncu R. The lysosome at the intersection of cellular growth and destruction. Dev Cell 2020; 54: 226–38.

Stuart JM, Segal E, Koller D, Kim SK. A gene-coexpression network for global discovery of conserved genetic modules. Science 2003; 302: 249–55.

Thomas JL, Vihtelic TS, denDekker AD, Willer G, Luo X, Murphy TR, et al. The loss of vacuolar protein sorting 11 (vps11) causes retinal pathogenesis in a vertebrate model of syndromic albinism. Invest Ophthalmol Vis Sci 2011; 52: 3119–28.

Uversky VN. The alphabet of intrinsic disorder: II. Various roles of glutamic acid in ordered and intrinsically disordered proteins. Intrinsically Disord Proteins 2013; 1: e24684.

van Dam S, Craig T, de Magalhaes JP. GeneFriends: a human RNA-seq-based gene and transcript co-expression database. Nucleic Acids Res 2015; 43: D1124–32.

Villegas F, Lehalle D, Mayer D, Rittirsch M, Stadler MB, Zinner M, et al. Lysosomal signaling licenses embryonic stem cell differentiation via inactivation of Tfe3. Cell Stem Cell 2019; 24: 257–70.

Yang M, Liu E, Tang L, Lei Y, Sun X, Hu J, et al. Emerging roles and regulation of MiT/TFE transcriptional factors. Cell Commun Signal 2018; 16: 31.

Zhang J, Lachance V, Schaffner A, Li X, Fedick A, Kaye LE, et al. A founder mutation in VPS11 causes an autosomal recessive Leukoencephalopathy linked to autophagic defects. PLoS Genet 2016; 12: e1005848.

Zhen Y, Li W. Impairment of autophagosome-lysosome fusion in the buff mutant mice with the VPS33A(D251E) mutation. Autophagy 2015; 11: 1608–22.